IN-SITU STUDY OF REVERSED AUSTENITE AND TRIP EFFECT OF A Ti STABILIZED SUPERMARTENSITIC STAINLESS STEEL

Julian David Escobar [1,2], Guilherme Faria [1,2], Leonardo Wu [1],
Paulo Roberto Mei [2], Antonio J. Ramirez [1,2]

[1] Brazilian Nanotechnology National Laboratory - LNNano - CNPEM, P.O. Box 6192, Campinas, SP, 13083-970, Brazil.
[2] School of Mechanical Engineering, University of Campinas – FEM - Unicamp, Campinas, SP, 13083-860, Brazil.

KEY WORDS: In-situ X-ray Diffraction, Reversed austenite, Supermartensitic stainless steel, TRIP effect.

The austenite fraction during heating, soaking, cooling and room temperature straining of a 12Cr-6Ni-2Mo-0.13Ti supermartensitic stainless steel (SMSS) were tracked using in-situ X-ray diffraction. The samples were heated at 10 °C.min^{-1}, up to 625 °C and 650 °C, kept during 9000 s and immediately cooled down to room temperature at 300 °C.min^{-1}. Results were compared to ex-situ intercritial tempering, showing similar microstructure, phase fractions and hardness. Subsequently an ex-situ double tempered sample was submitted to cold straining, tracking the γ_{rt} to M transformation. The strain induced transformation started after surpassing the yield strength of the material. During the first part of the plastic deformation, it was seen a fast γ_{rt} to M transformation. At the end of the plastic region, almost all the γ_{rt} was consumed. The in-situ measurements were performed at the X-Ray scattering and thermo-mechanical simulation experimental station (XTMS) managed by the Brazillian National Nanotechnology Laboratory (LNNANO), which is installed at the Brazilian Synchrotron Light Laboratory (LNLS). The XTMS installation consist of a diffraction beamline built around an advanced thermo-mechanical simulator, which allows the material of interest to be submitted to a wide range of thermo-mechanical conditions with high accuracy and reproducibility.

julian.escobar@lnnano.cnpem.br – DEMA-FEM-UNICAMP, Rua Mendeleiev, s/n - Cidade Universitária Zeferino Vaz, Campinas, SP, 13089-970, Brazil. +55(19)35175085

antonio.ramirez@lnnano.cnpem.br- LNNano-CNPEM, P.O. Box 6192, Campinas, SP, 13083-970, Brazil. +55(19)3518-3108

1. Introduction

Commercially, supermartensitic stainless steels (SMSS) are provided to the oil and gas industry with a balanced microstructural combination of tempered

Martensite (α'), reversed austenite (γ_{rt}) and little or no presence of δ ferrite [1-4]. Offshore service specifications, corrosion standards and manufacturers suggest a maximum in service hardness of 281 HV. To satisfy this technical requirement, simple or double temperings slightly above the A_{c1} transformation temperature should be carried out in order to reduce hardness by reverting and retaining austenite at room temperature. Typically, the γ_{rt} phase content ranges between 10% and 25%, and its beneficial influence is related to the overall hardness reduction and to transformation induced plasticity (TRIP effect) from γ_{rt} to M [5, 6]. Nevertheless, this heat treatment must be carefully designed to keep yield strength above 500 MPa so as to represent a cost benefit over duplex stainless steels in mild sour and sweet corrosive environments [2, 4].

Many researchers have studied the response of SMSS after intercritical temperings after furnace heat treatments [5, 7, 8, 9]. Results showed that for each alloy design, there is a temperature of maximum γ_{rt} retention. Below and above that temperature, retention decreases by two reasons. First, by low production of stable austenite; and second, by excessive production of unstable austenite. In-situ high temperature XRD experiments allowed quantifying the fraction of each phase at the end of the isothermal stage [9, 10]. However, obtaining conventional diffraction data is a time consuming experience which can take several hours with standard equipment, which decreases the accuracy of in-situ XRD analysis because the transformation kinetics is still ongoing during measurements.

In-situ X-ray diffraction by synchrotron radiation is a powerful technique to study phase transformations [11, 12]. Linear or area X-ray detectors are used for fast data acquisition, permitting time resolved measurements. This allows tracking phase transformation kinetics during thermomechanical simulation with a time resolution around second. In the present work, In-situ studies of phase transformation kinetics during austenite reversion and TRIP effect of a Ti-stabilized supermartensitic stainless steel were conducted. Dilatometry, hardness, phase fractions and microstructures were compared to furnace heat treated samples to validate the in-situ thermomechanical simulation.

2. Experimental Procedure

2.1 Base material

A highly alloyed supermartensitic stainless steel (SMSS) stabilized with Ti with chemical composition shown in table 1 was used in this study. For this compositional range, it is expected that all the austenite formed during heat treatments above A_3 will completely transforms to fresh Martensite when subjected to any engineering cooling rate [3]. The Ti is added to capture C and N enhancing ductility and weldability, and to control hardening at the HAZ during arc welding.

As-received plates of 6 mm x 50 mm x 100 mm subjected to hot rolling and annealing presented hardness, microstructure, and phase fractions quite different from the quenched and tempered condition commonly used by the oil and gas industry. Before dilatometric and ex-situ heat treatment experiences, samples were previously submitted to austenitization at 1050 °C during 30 minutes, followed by air-quenching.

Throughout this work, γ is used to arbitrarily refer to the austenitic phase; γ_t is the percentage of austenite reversed (formed) at a specific temperature during the heat treatment; and γ_{rt} is the percentage of reversed austenite present at room temperature after cooling from an intercritical tempering.

Table 1. Chemical composition (wt-%) of a UNS S41426 Supermartensitic Stainless Steel.

C	N	Si	Mn	P	S	Ni	Cr	Mo	Cu	Ti	V
0,024	0,0129	0,26	0,48	0,027	0,002	5,9	12,02	1,93	0,09	0,13	0,04

2.2 Dilatometry and Ex-situ heat treatments

Dog-bone type samples with 8 mm long reduced section and 5 mm x 5 mm central cross section were used for the dilatometric tests. A joule heating Gleeble 3800® thermomechanical simulator coupled with a contact dilatometer was used. In this system, the direct resistive heating is controlled using a type K thermocouple directly attached to the sample. Heating and cooling rates of 10° C.min^{-1} were used to measure A_{c1}, A_{c3}, M_s and M_f temperatures.

For the ex-situ heat treatments the samples were put inside the furnace 100 °C before it reached the sought temperature. After 9000 seconds, samples were cooled in standing air to room temperature. Two intercritical tempering temperatures were selected for the isothermal treatments: 625 and 650 °C.

2.3 In-situ thermal and mechanical simulation

The present measurements involve heating, soaking, cooling and cold straining of samples at the X-Ray scattering and thermo-mechanical simulation experimental station (XTMS), installed at the XRD1 beamline at the Brazilian National Synchrotron Source (LNLS). The incident beam energy used was 10 keV. The beam size was controlled by slits and set to 0.5 mm high and 2.0 mm wide. Samples were heat treated using the direct resistive heating method, controlled by type K thermocouples. This method causes a temperature gradient around the tested area, but temperature variation on the gauge volume is negligible. A linear detector with 0.05° angular resolution was used to collect diffraction from a partial region (32 to 42°) involving {111}γ, {200}γ and {110}α' families of planes. In order to reduce oxidation during in-situ experiences, pressure in the sample chamber was set to 10^{-3} torr.

Flat dog-bone shaped samples with 2 mm thick, 5 mm wide and 20 mm long reduced section were used. Due to the mechanical instability of the γ_{rt} phase, the sample facet used for the diffraction measurements were grinded and polished to 1 μm to minimize deformation at the surface. Samples were heated at 10 °C.min^{-1} to 625 and 650 °C and held at these temperatures during 9000 seconds, and then cooled at a rate of 300 °C.min^{-1} to simulate air-cooling conditions. During heating and soaking, data was collected each 30 seconds to maximize signal to noise ratio. It was possible to track phase transformations during heating with a thermal resolution of 5 °C. During cooling, data was collected every 3 seconds, which

mean data averaging over 10 ℃. Cold straining was conducted at a constant rate ($\dot{\varepsilon} = 4\text{x}10^{-5}\text{s}^{-1}$) until rupture. Diffraction data was continuously collected every 30 seconds.

2.4 Microstructural characterization and quantitative phase fraction measurements

Microhardness, conventional Co Kα x-ray diffraction (XRD) and optical microscopy (OM) were used to characterize the as-received, heat treated, and thermo-mechanically simulated samples. The metallographic preparation consisted on conventional grinding and polishing down to 0,25 μm diamond paste. The microstructure was analyzed after etching with Vilella's reagent for 10-30 s in order to reveal prior-austenitic grain boundaries and the tempered Martensite. Vickers microhardness (HV0.2/15s) was also used to evaluate the different microstructural conditions.

The austenite volume fraction at room temperature, as well as during thermal and mechanical simulation was evaluated using equation 1, by measuring the integrated intensities of {111}γ, and {110}α' planes. For simplicity, it was assumed that the carbide fraction was irrelevant when compared to α' and γ fractions, (equation 2) [9].

$$V_\gamma = \frac{1{,}4I_\gamma}{I_{\alpha'} + 1{,}4I_\gamma} \quad \text{(eq. 1)}$$

$$V_\gamma + V_{\alpha'} = 1 \quad \text{(eq. 2)}$$

Where, V_γ and $V_{\alpha'}$ are the volume fractions of austenite and tempered Martensite, respectively, and Iγ and Iα' are the integrated intensities of {111}γ, and {110}α', respectively.

3. Results and Discussion

3.1 Base material characterization

Figure 1 a shows the material in the as-received condition, ie. after hot forming and annealing. The microstructure consists in a typical low carbon lath Martensite and a small fraction of fine Ti (C, N) particles. δ ferrite was not found after metallographic inspection by using Sulphuric and Stock reagents [1]. To proceed with the austenite reversion process, and in order to bring the material to a known condition, the samples were austenitized at 1050 ^{o}C for 30 min, followed by air-quenching. Similar to the as-received material, the obtained microstructure consisted of M and Ti (C, N). Due to the elevated hardenability of SMSS, it is expected complete the γ → M transformation when annealed or air-quenched. After quenching (figure 1 b), it was observed an increment in the lath size when compared to the as-received condition (figure 1 a). This is explained by the additional austenitizing process at 1050 ℃ for 30 min.

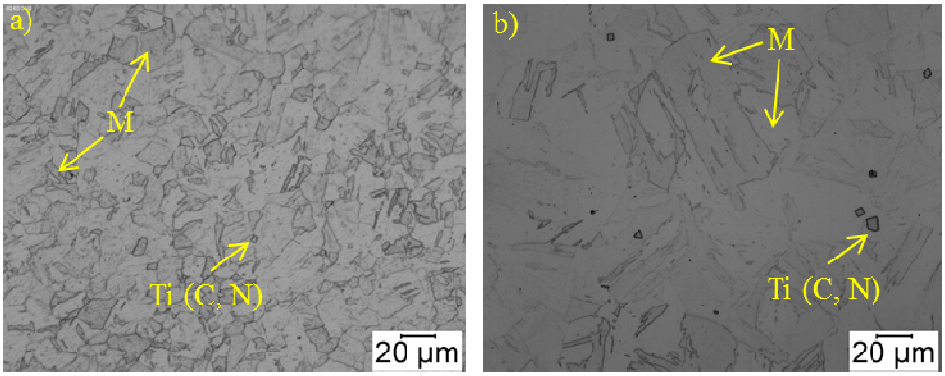

Figure 1. Microstructure of a highly alloyed Ti stabilized SMSS in the a) as-received condition, b) Austenitized and air-quenched condition. OM.

Dilatometric examinations shown in figure 2 were conducted during heating and cooling at 10 °C.min^{-1} to determine the start temperature for the α' → γ transformation (A_{c1}), the γ formation finish temperature (A_{c3}), the Martensite transformation start temperature (M_s) and finish temperature (M_f).

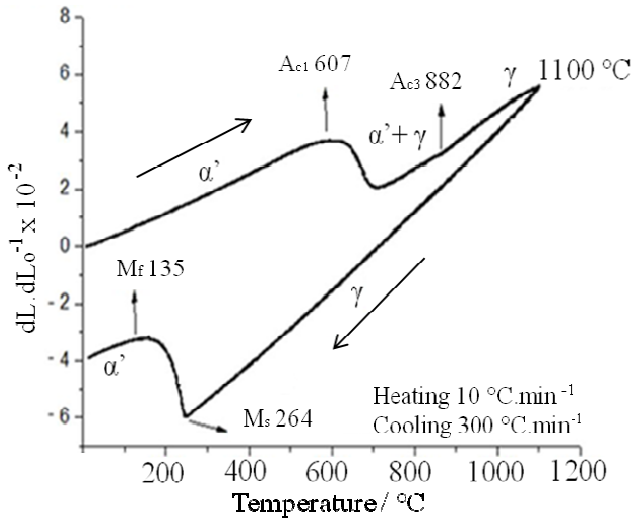

Figure 2. Dilatometric examinations for an air-quenched highly alloyed SMSS during heating and cooling at 10 °C.min^{-1} from 1100 °C.

The A_{c1} and A_{c3} temperatures were found at 607 ± 8 °C and 882 ± 5 °C, respectively. This A_{c1}-A_{c3} region represents the biphasic α' - γ field, where intercritical temperings have to be conducted to reverse γ_{rt}, especially in temperatures slightly above A_{c1} [4-9]. During cooling, the first transformation corresponding to M_s temperature, was observed at 264 ± 14 °C. The Martensitic transformation continues until reaching the M_f temperature at 127 ± 6 °C. Knowing the A_{c1} temperature, it was possible to specify two intercritical tempering temperatures: 625 °C and 650 °C, were the following heat treatments were performed.

3.2 Furnace intercritical tempering

As stated above, intercritical tempering treatments were performed at 625 and 650 ℃ for 9000 s (150 min.), which were followed by air cooling. The heat treated samples had a microstructure formed by α' matrix with Ti (C, N), as presented in figure 3, and finely dispersed γ_{rt}, measured by XRD. The ex-situ XRD analysis revealed less intense γ_{rt} peaks for the sample subjected to intercritical tempering at 650 ℃ when compared to the one subjected to heat treatment at 625 ℃. This is explained by the larger fraction of γ_t formed during the isothermal stage of the tempering at 650 °C. Reversed austenite retention at room temperature depends on the phase chemical composition achieved during the intercritical treatment through diffusion of austenite stabilizing elements (C, N, Mn, Si and Ni) from the α' matrix [5, 6, 9, 10]. If the treatment conditions are such that γ_t is enriched in the above mentioned elements, M_s and M_f temperatures are reduced, resulting on the retention of the more stabilized austenitic grains. As a relevant fraction of the C and N are associated to the Ti (C, N) particles, even at such low temperatures, Ni enrichment may be playing an important role on the γ_t stabilization and therefore in the γ_{rt} retention [9]. Therefore, during a heat treatments at higher temperatures, ie. 650 ℃, a larger fraction of γ_t is formed, compromising its enrichment on gamma stabilizing elements, reducing final γ_{rt} fraction at room temperature.

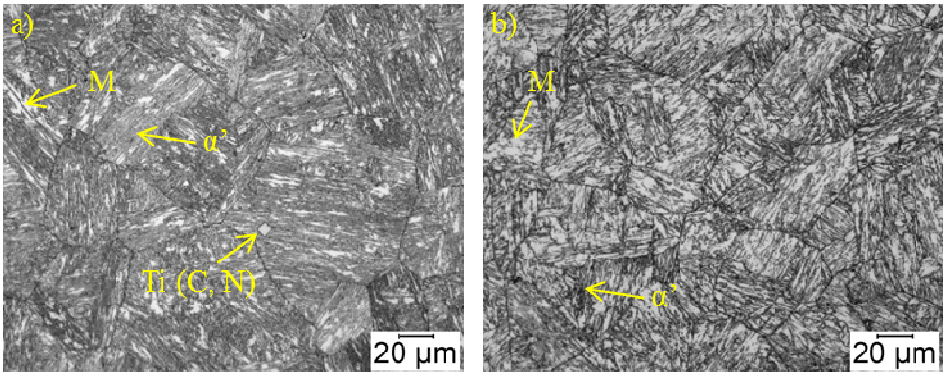

Figure 3. Microstructure after quenching and tempering of a highly alloyed Ti-stabilized SMSS during 9000 s at, a) 625 ℃, b) 650 ℃. OM. Vilella's Reagent.

Phase fraction quantification analysis plotted in figure 4, showed 14 and 5 % of γ_{rt} after air cooling from 625 and 650 ℃, respectively. Despite the difference in the γ_{rt} fraction, hardness values remained similar, 281±6 and 284±11 HV0.2/15s, respectively. However, these hardness values are lower than those found in the as-received (301±7 HV0.2/15s) and austenitized + air-quenched conditions (301±11 HV0.2/15s). No discernible austenite peaks were observed in the as-received and austenitized + air-quenched samples.

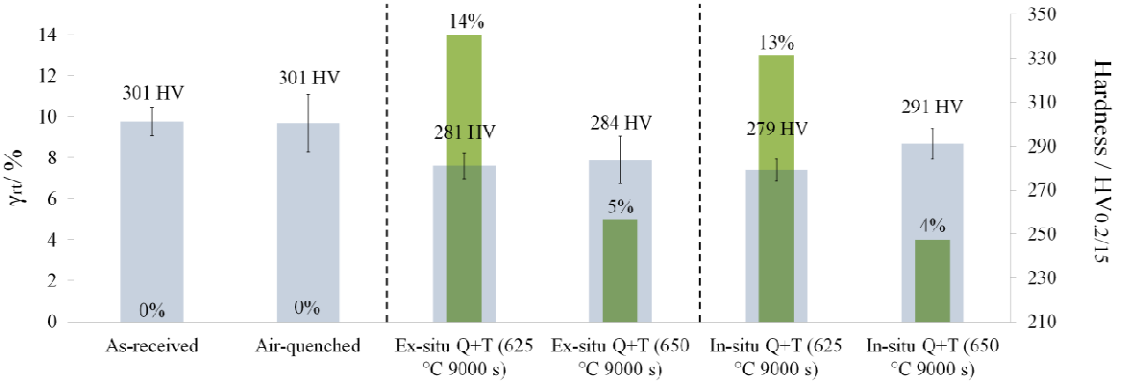

Figure 4. Reversed austenite fraction (%vol) and hardness of a highly alloyed SMSS after different heat treatment conditions.

3.3 In-situ thermal and mechanical simulation

A second set of experiments was performed to better understand the intercritical tempering process. For such, the phase transformations kinetics during heating, soaking, cooling, and cold straining were monitored with in-situ time-resolved X-ray diffraction at the XTMS beam station. Leem, et al. [9], have shown that the α'→γ transformation is diffusion controlled when the sample is heated at rates up to 10 ℃.s^{-1} (60 ℃.min^{-1}). Therefore, a heating rate of 10 ℃.min^{-1}, similar to dilatometric examinations, was selected. The diffraction results from the simulated intercritical tempering treatments performed at 625 and 650 °C are summarized in figures 5.a and 5.b, respectively. The figure presents single data acquisition spectra acquired at known time and temperature. During the experiments were collected more spectra than the ones plotted, but for simplicity the figure presents just some of them. However, even all this data was examined for quantitative analysis. These data allows to track the austenite and Martensite volumetric fraction evolution by evaluating the {111}γ, {200}γ and {110}α' families of peaks. The three stages of these heat treatments, heating, soaking, and cooling can be easily differentiated:

- During the heating stage, fresh Martensite suffers a gradual tempering process, producing a classic parallel needle-like structure inside packages, within the martensitic grains [1, 9]. The {110}α' peak shift to the left during the heating process is due to the thermal expansion. The starting temperature for the austenite formation, A_{c1}, was measured for both experiments to be 620 ± 5 ℃, as indicated by the gay lines, which is in good agreement with the dilatometric examinations. Figure 6.a shows the γ_t volumetric fraction as a function of temperature during heating. When the samples reached the isothermal intercritical tempering temperature, a small fraction of γ_t has already formed, being 0,6 and 4,5 %vol at 625 and 650 ℃, respectively.

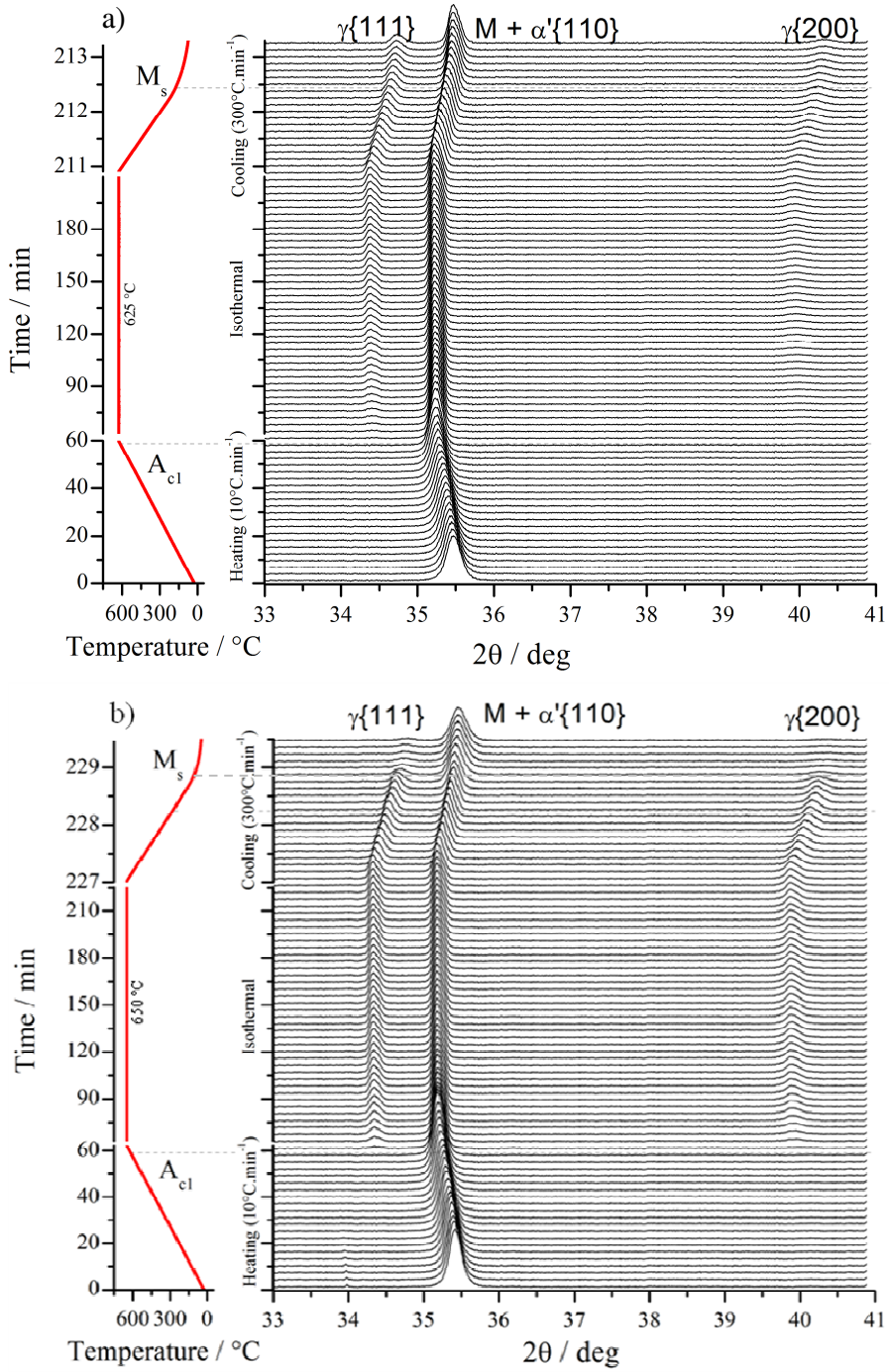

Figure 5. Time-resolved synchrotron X-ray diffraction data from samples subjected to 3 stage in-situ thermal simulation: 1. Heating at 10 °C.min^{-1}; 2. intercritical tempering at a) 625 °C, and b) 650 °C during 9000 s; and 3. Cooling to room temperature at 300 °C.min^{-1}.

- During the soaking stage, the temperature was kept constant at 625 or 650 °C during 9000 seconds, while the isothermal phase transformation kinetics was recorded. It was possible to observe a continuous increase on the {111}γ

and {200}γ peak intensities. This behaviour was more accentuated for the 650 °C treatment, showing that temperature has a more relevant influence on the isothermal α' to γ_t transformation than time, for the studied conditions. This behaviour specially evident on the {200}γ peak. Quantitative results shown in figure 6.b present isothermal transformation process, which has a more accentuated kinetics at the beginning of the transformation at 650 °C. At this higher temperature, 23%vol of γ_t has been formed during 800 s soaking, whereas only 6% has formed at 625 °C. At the end of the isothermal stage, the phase fractions were 32%vol γ_t + 68%vol α' at 625 °C, and 46%vol γ_t + 54%vol α' at 650 °C.

- During the cooling stage is possible to observe the peaks shift to the right due to the thermal contraction. The Ms temperature was identified for both experiments, as indicated by the gay lines. Despite the higher intensity of the austenite peak, it can be noticed that the martensitic transformation is more accentuated for the sample heated to 650 °C. At the end of the cooling process for the sample heated to 650 °C, the γ_{rt} peaks can barely be noticed. After the martensitic transformation starts, {110} peak is formed by the unchanged α' fraction and the fresh martensite fraction transformed from the unstable γ_t. Transformation was tracked until reaching 50 °C, and a final acquisition was made after few minutes at room temperature. Quantitative results plotted in figure 6.c show Ms temperatures, of 170 and 290 °, indicated as the first inflection points for the 625 and 650 °C experiment curves, respectively. When cooling from 625 °C, the austenite stabilization at lower temperatures is evident. To quantify this behaviour, an austenite stability factor f_γ defined by the authors in equation 3, can be introduced:

$$f_\gamma = \frac{\gamma_{rt}}{\gamma_t} \quad \textit{(eq. 3)}$$

Where, γ_{rt} is the reversed austenite fraction at room temperature, and γ_t austenite fraction formed at the end of the isothermal (intercritical) stage. The austenite stability (f_γ = 0.4) is higher for the sample treated at 625 °C, when compared to the one treated at 650 °C (f_γ = 0.1), bringing the Martensitic transformation to lower temperatures, for the lower temperature tempering treatment. Consequently, the γ_{rt} fraction at room temperature was 14%vol and 4%vol for the samples tempered at 625 °C and 650 °C, respectively, as presented in figure 4. This volumetric fractions and the resultant hardness values are in very good agreement with the furnace ex-situ heat treatments results. Table 2 summarizes the transformation temperatures, phase fractions and austenite stability measured using the situ X-ray diffraction experiments.

The microstructures of the thermally simulated samples, shown in figure 7, are alike to those observed on the samples subjected to ex-situ furnace heat treatments. The sample treated at 625 °C, figure 7.a, presentes α' matrix with 19%vol M and 13%vol γ_{rt}. However, for the sample treated at 650 °C, figure 7.b, the M content has risen to 42%vol, causing a reduction in both α' matrix and $\gamma_{rt.}$ to 54% and 4%, respectively.

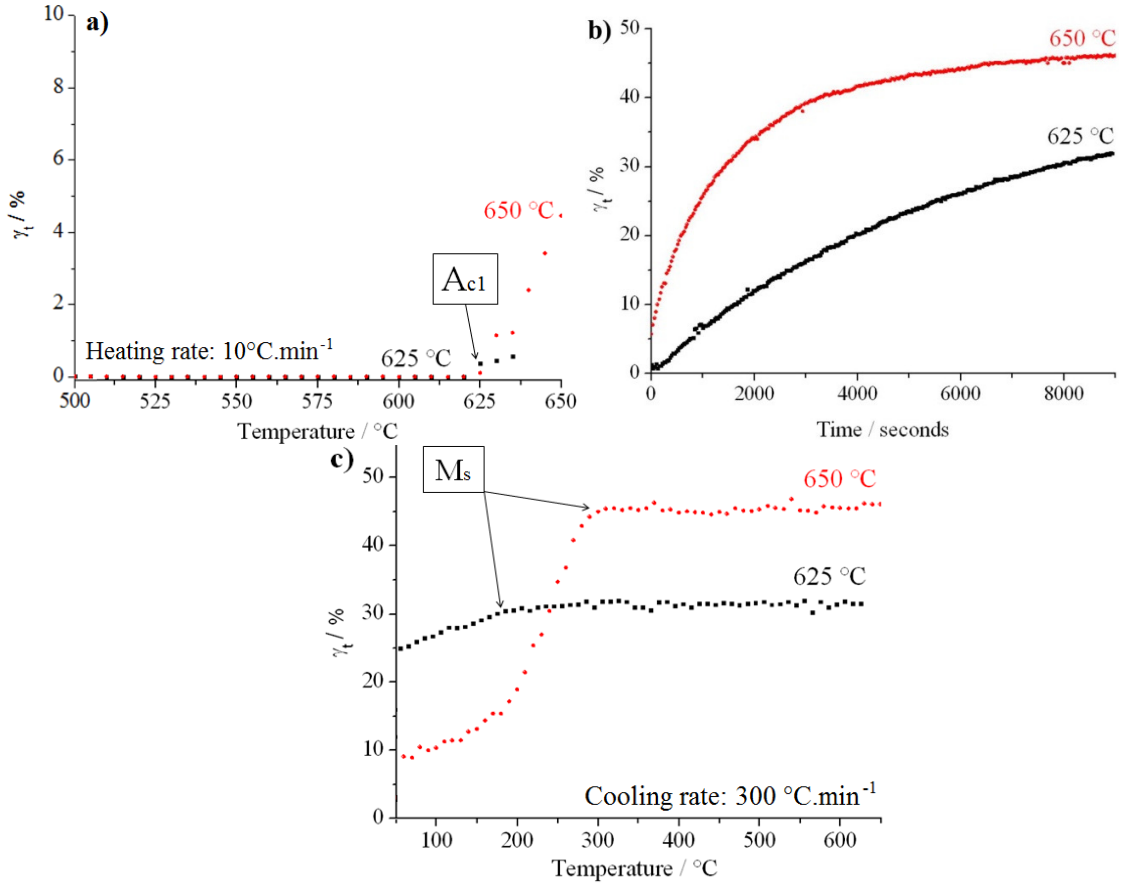

Figure 6. Austenite fraction (%vol) evolution during time-resolved synchrotron X-ray diffraction experiments from samples subjected to 3 stage in-situ thermal simulation: a) Heating at 10 °C.min^{-1}; b) Intercritical tempering at 625 and 650 °C during 9000 s; and c) cooling to room temperature at 300 °C.min^{-1}.

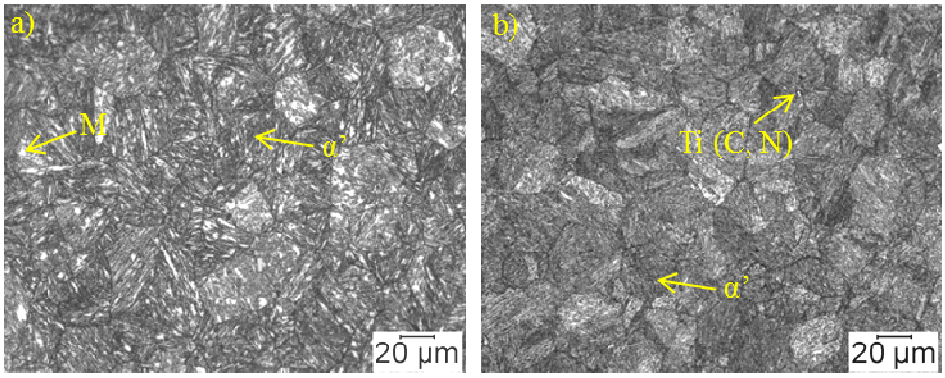

Figure 7. Microstructure after in-situ intercritical tempering of a highly alloyed Ti-stabilized SMSS during 9000 s at, a) 625 °C, b) 650 °C. OM. Vilella's Reagent.

Table 2. Phase transformation temperatures, phase fraction (%vol) and austenite stability (f_γ) obtained by time-resolved in-situ X-ray diffraction analysis of highly alloyed Ti-stabilized SMSS.

Temperature / °C	Transformation temperature / °C				Phase percentage / %				
	A_{c1}	A_{c3}	M_s	M_f	γ_t	γ_{rt}	M	α'	f_γ
625	625	-	170	-	32	13	19	68	0.4
650	625	-	290	-	46	4	42	54	0.1

Another sample was austenitized + air-quenched, and subjected to ex-situ double tempering at 670 °C during 2 hours, and 630 °C during 5 hours to obtain a tempered Martensite matrix with finely dispersed γ_{rt}. After such heat treatment, the material was submitted to an in-situ uniaxial tension test at constant strain rate of $\dot{\varepsilon} = 4\text{x}10^{-5}s^{-1}$ to study the strain induced transformation (TRIP effect) of γ_{rt}. The results are shown in figure 8. Diffraction spectra was recorded every 30 seconds.

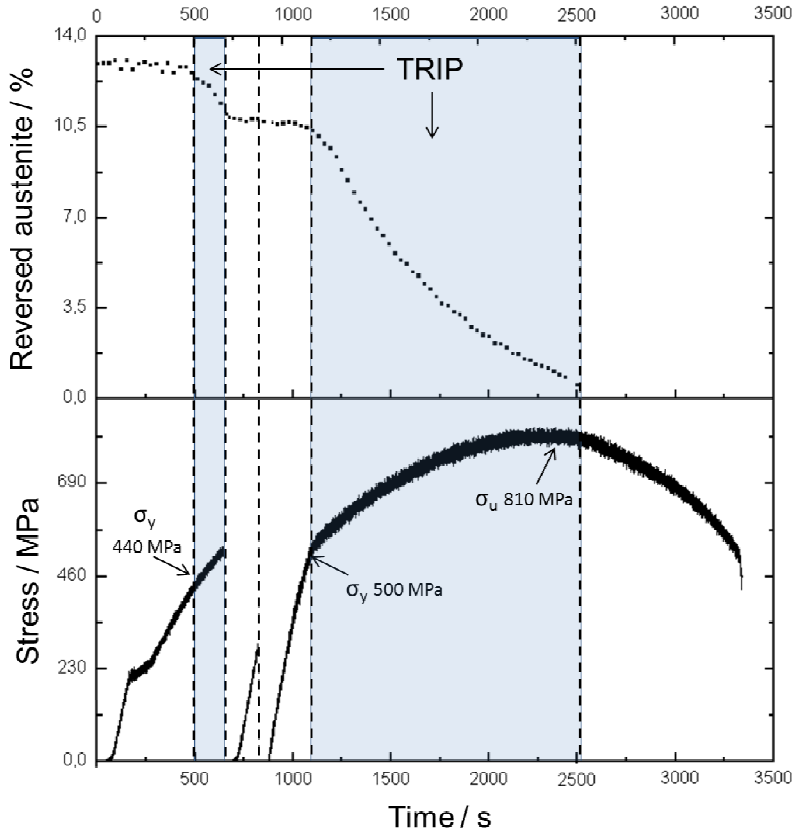

Figure 8. Time-resolved in-situ X-ray diffraction study of γ_{rt} TRIP effect of a double quenched SMSS sample submitted to uniaxial room temperature straining at a constant rate of $\dot{\varepsilon} = 4\text{x}10^{-5}s^{-1}$.

The strain induced martensitic transformation only started when yield strength was reached at 440 MPa at the first straining stage. The sample was completely unloaded after 500 MPa, and subsequently stressed to 250 MPa to verify the absence of TRIP effect during the elastic regime. A third loading cycle was started after 3% γ_{rt} to M transformation. During the initial stage of the plastic deformation, constant work hardening can be observed, accompanied by a fast γ_{rt} to M phase transformation. In this case, the yield strength was raised to 500 MPa. According to other authors [6, 13], the first austenitic grains to transform are the less chemically stabilized, and the less geometrically restricted ones, generally located at grain boundaries. The most stable γ_{rt} will help the material to avoid flow instabilities, as long as these are homogeneously and finely dispersed in the tempered Martensite matrix (α'). Almost all the γ_{rt} was consumed, before reaching the tensile strength. Thus, during the necking process no austenitic peaks could be detected.

Satisfactory results of in-situ time resolved x-ray diffraction during cold straining were obtained. Further studies using different straining rates and temperatures can be performed at the XTMS installation, in order to clarify the influence of these parameters during TRIP effect.

5. Conclusions

- It was possible to track the transformation kinetics during the thermo-mechanical simulation of a highly alloyed Ti-stabilized supermartensitic stainless steel by means of time-resolved X-ray diffraction techniques using synchrotron radiation. Simulated intercritical tempering treatments satisfactorily reproduced the microstructure, hardness, and phase fractions of common furnace heat treatments. Phase transformation temperatures were also in very good agreement with those found during dilatometric experiences.
- Lower intercritical tempering temperatures should be used in order to maximize the γ_{rt} fraction in the α' matrix, and to minimize the γ_{rt} to M transformation during cooling to room temperature.
- Intercritical tempering temperatures slightly superior to A_{c1} are better to revert, stabilize and retain austenite at room temperature. At 625 ℃, it is possible to revert up to 14 % of γ_{rt} with a stability factor of 0.4. At 650 ℃, there is acceleration of the transformation kinetics from α' to γ_t; but simultaneously, a reduction in the austenitic stability factor to 0.1, resulting in only 4% of γ_{rt} after cooling to room temperature.
- It was possible to track the strain induced $\gamma_{rt} \rightarrow$ M transformation by means of time/stress/strain-resolved in-situ X-ray diffraction monitoring during a uniaxial room temperature strain test. The $\gamma_{rt} \rightarrow$ M transformation started after reaching the yield strength, evolving up to the tensile strength and ending just after the beginning of the necking process.

6. Acknowledgements

The authors acknowledge CPM/LNNano/CNPEM for the technical support during insitu x-ray experiments (XTMS beam line at LNNano-LNLS/CNPEM) microscopy, XRD and dilatometric experiences; Villares Metals S.A. for the SMSS donation; Petrobras for the financial support; CAPES for the scholarships; and UNICAMP for the academic support.

7. References

1. CARROUGE, D.; BHADESHIA, H. K. D. H.; WOOLLIN, P. Effect of δ-ferrite on impact properties of supermartensitic stainless steel heat affected zones. Science and Technology of Welding and Joining, v.9, p.377-389, 2004.
2. LANGE, H. et al. Material Selection of Weldable Super Martensitic Stainless Steel for Linepipe Materials. SINTEF Materials and Chemistry. Marintek, Agosto, 2004. www.sintef.no
3. KONDO, K.; UEDA, M.; OGAWA, K.; AMAYA, H.; HIRATA, H.; TAKABE, H. Alloy Design of Super 13 Cr Martensitic Stainless Steel (Development of Super 13 Cr Martensitic Stainless Steel for Line Pipe). In: Supermartensitic Stainless Steels '99', p. 11–18, Belgium, 1999.
4. KONDO, K.; AMAYA, H.; OHMURA, T.; MORIGUCHI, K. Effect of cold work on retained austenite and on corrosion performance in low carbon martensitic stainless steels. In: Corrosion 2003. Paper 0394, Houston, Texas, 2003.
5. BILMES, P.D.; SOLARI, M.; LLORENTE, C.L. Characteristics and Effects of Austenite Resulting from Tempering of 13Cr-NiMo Martensitic Steel Weld Metals. Materials Characterization, v. 46, p. 285-296, 2001.
6. KARLSEN, M.; HJELEN, J.; GRONG, Ø.; RØRVIK, G.; CHIRON, R.; SCHUBERT, U. The stability of retained austenite in supermartensitic stainless steel (SMSS) examined by means of SEM/EBSD. In: EMC 2008 14th European Microscopy Congress 1–5 September 2008, Aachen, Germany, pp 561-562, 2008.
7. ZOU, D.; HAN, Y.; ZHANG, W.; FANG, X. Influence of Tempering Process on Mechanical Properties of 00Cr13Ni4Mo Supermartensitic Stainless Steel. Journal of Iron and Steel Research, International, v.17, p. 50-54, 2010.
8. MA, X.P.; WANG, L.J.; LIU, C.M.; SUBRAMANIAN, S.V. Microstructure and properties of 13Cr5Ni1Mo0.025Nb0.09V0.06N supermartensitic stainless steel. Materials Science and Engineering A, v. 539, p.271-279, 2012.
9. LEEM, D.; LEE, Y.; JUN, J.; CHOI, C. Amount of retained austenite at room temperature after reverse transformation of Martensite to austenite in an Fe-13%Cr-7%Ni-3%Si martensitic stainless steel. Scripta Materialia, v. 45, p. 767-772, 2001.
10. BOJACK, A.; ZHAO, L.; MORRIS, P.F.; SIETSMA, J. In-situ determination of austenite and Martensite formation in 13Cr6Ni2Mo supermartensitic stainless steel. Materials Characterization, v.71, p.77-86, 2012.
11. ZHANG, S.; TERAZAKI, H.; KOMIZO Y. In-situ Observation of Martensite transformation and retained austenite in supermartensitic stainless steel. Transactions of JWRI, v. 39, 2010.
12. BABU, S.S.; SPECHT, E.D.; DAVID, S.A.; KARAPETROVA, E.; ZSCHACK, P.; PEET, M.; BHADESHIA, H.K.D.H. In-situ observations of lattice parameter fluctuations in austenite and transformation to bainite. Metalurgical and materials transactions A, v. 36A, 2005.
13. GARCIA-MATEO, C.; CABALLERO, F.G.; SOURMAIL, T.; KUNTZ, M.; CORNIDE, J.; SMANIO, V.; ELVIRA, R. Tensile behavior of nanocrystalline bainitic steel containing 3 wt% silicon. Materials science and engineering A, v.549, p. 185-192, 2012.